

Monolithic Design and Fabrication of a 2-DOF Bio-Inspired Leg Transmission

Daniel M. Aukes, Onur Ozcan, and Robert J. Wood *

School of Engineering and Applied Sciences
Wyss Institute for Biologically Inspired Engineering
Harvard University, Cambridge MA.

Abstract. We present the design of a new two degree-of-freedom transmission intended for micro / meso-scale crawling robots which is compatible both with laminate manufacturing techniques and monolithic, “pop-up” assembly methods. This is enabled through a new design suite called “popupCAD”, a computer-aided design tool which anticipates laminate manufacturing methods with a suite of operations which simplify the existing design workflow. The design has been prototyped at three times the anticipated scale to better understand the assembly and motion kinematics, and simulated to establish the basic relationships between the actuator and end-effector transmission ratios.

1 Introduction

The advent of new laminate-manufacturing techniques such as Printed-Circuit MEMS (PC-MEMS) [9, 10], Smart Composite Micro-structures (SCM) [6, 11], and Lamina Emergent Mechanisms (LEM) [4, 8] has enabled the development of a new class of millimeter-scale devices. These manufacturing techniques use a relatively small set of operations such as cutting, lamination, and folding to create a variety of mechanical components, such as hinges, structural elements, and springs. These devices are typically designed through the selective removal of material across neighboring material layers to create planar mechanisms. By using multiple materials in the laminate, the mechanical properties of these devices can be tuned for each component. Highly specialized devices can be developed through the iterative use of these operations, and discrete components can be added throughout the process. Using laser cutters to create precise alignment geometry, highly complex kinematics can also be created between hinged rigid bodies and utilized both for structures and mechanisms.

Through these new manufacturing techniques, a variety of new devices have been realized, from flying micro-robots inspired by bees [10] to crawling robots

* This material is based upon work supported by the National Science Foundation (grant numbers EFRI-1240383 and CCF-1138967) and the Wyss Institute for Biologically Inspired Engineering. Any opinions, findings, and conclusions or recommendations expressed in this material are those of the authors and do not necessarily reflect the views of the National Science Foundation.

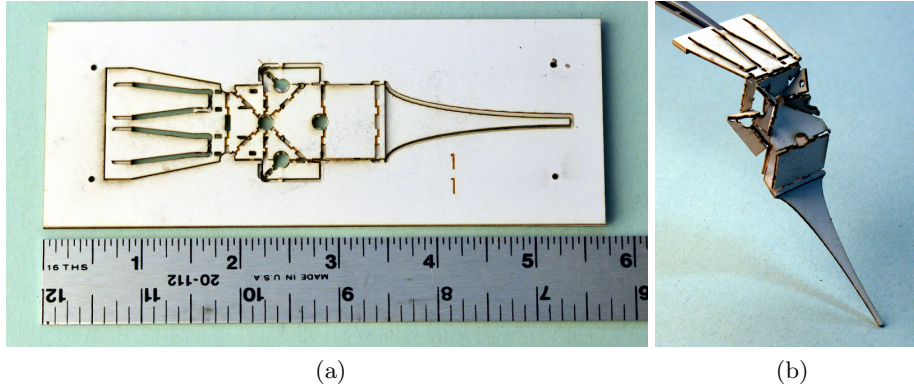


Fig. 1: Prototype transmission in (a) flattened and (b) assembled configurations.

[2, 3, 7]. In addition, [9] demonstrates monolithic assembly techniques for faster, more precise manufacturing with a device called “Mabee”. For all the potential of this concept, however, only this device has used monolithic “pop-up” fabrication techniques. This is due in part to the lack of design software which encapsulates laminate design and manufacturing rules; consequently the addition of assembly scaffolds adds too much complexity to the average design. To work around such complexities, designers split devices into simpler parts, ultimately relying on manual assembly and locking operations which require dexterity and expertise. Thus, manufacturing remains slow and error-prone.

In order to facilitate the transition from manual manufacturing of discrete components to more automated, monolithic fabrication of entire robots, we present preliminary work on a bio-inspired, two degree-of-freedom transmission to be used in the leg of a crawling robot, which is compatible with the concepts of PC-MEMS manufacturing and monolithic, “pop-up” assembly. This design is composed entirely of elements which begin flat and pre-assembled in a laminate, and by actuating and locking a single degree of freedom, are positioned into their assembled state.

2 Device Overview

The motion of cockroach and centipede legs in robotic systems is often approximated as a two-degree-of-freedom system (lifting the foot up and down, and swinging the foot forward and backward). We have previously built robots inspired from these organisms using PC-MEMS fabrication methods with manual [5] or popup assembly techniques [3] that can achieve two-degree-of-freedom leg motion.

The device shown in Figure 2a consists of many individual linkages connected through hinges on two sub-laminate layers. These linkages are arranged around four spherical linkages: two six-bar rotational linkages (6R) and two four-bar

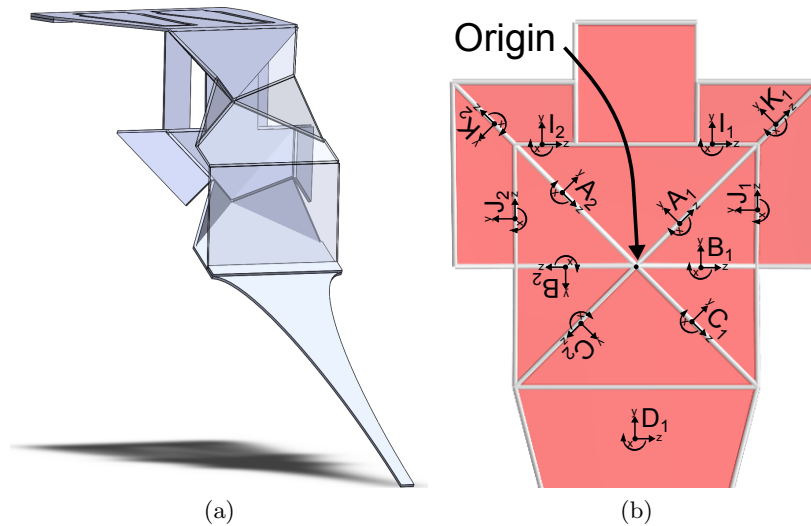


Fig. 2: The full leg design is shown in in (a). Links of the upper 6R spherical mechanism are translucent . Reference frames for the three linkages on the bottom sublaminates are shown in (b).

rotational linkages(4R). Both linkages start in their flattened state, but rotate in three-dimensional space about one point when actuated.

In combining the input and output stages of such linkages in various ways, interesting kinematic properties can be exploited. For example, the output stage of the 6R spherical linkage used in Figure 1 has the properties of a spherical joint, with three degrees of freedom in rotation. Two grounded spherical linkages whose output stages are rigidly connected, however, are more constrained in their motion, acting as a single degree-of-freedom rotational hinge. Similarly, four-bar linkages exhibit only a single degree of freedom between input and output stages, yet can impart highly nonlinear motion relationships between the two. Yet all these devices start flat and are thus compatible with PC-MEMS manufacturing processes, making them ideal building blocks for pop-up compatible designs.

In this design, the connection of these elementary building blocks mimics structures seen in biology. Multiple degrees of freedom can be seen in the human hip joint, for example, where ball-and-socket mechanisms in the bones and cartilage provide smooth rotation across a wide range of angles. Yet the motion of joints such as this is rarely constrained by a single mechanism but are complemented by a redundant set of muscles and tendons which route across and between joints, guiding, supporting and restricting motion. In this way, the leg mechanism, with its redundant-yet-constrained six bar linkages, provides a more-limited degree of motion than each subcomponent independently would be capable of delivering – and in a way which is inherently more manufacturable.

Parallels to this concept are prevalent in biological systems as well, where the capabilities of the integrated system are greater than the sum of its parts.

3 CAD Design, Fabrication, and Materials

The initial design of the device is carried out in Solidworks in order to test the design concept and perform initial kinematic simulations. However, the Solidworks design only includes basic sketches of the layers, and not detailed drawings of features. The actual design used for fabrication is done using a new Computer Aided Design and Manufacturing (CAD/CAM) application called popupCAD [1]. Traditional CAD/CAM software, such as Solidworks, does not have any built-in tools to help with unconventional manufacturing methods such as PC-MEMS or SCM. On the other hand, popupCAD is specifically designed for layer-based manufacturing methods. The software automatically generates cut files using PC-MEMS and Pop-Up MEMS design and fabrication rules. It also has several operations specific to layer-based design and fabrication methods (e.g. generating support structures around features). In order to take advantage of these software features, we have imported the Solidworks sketches into popupCAD as guidelines, completed the design by adding the necessary PC-MEMS features such as hinges and support web, and generated the cut files in popupCAD. An example initial cut file and the final cut file used to fabricate the device is shown in Figure 3.

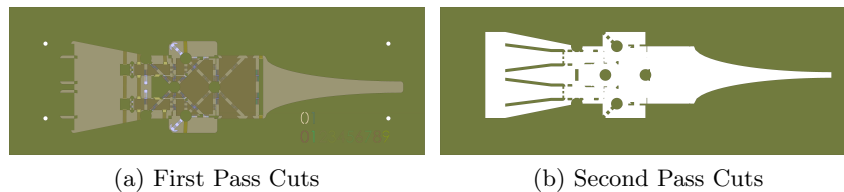


Fig. 3: First and Second Pass Cuts

The device is fabricated using SCM [6, 11] and Pop-Up Manufacturing / Assembly methods [9, 10], outlined in Figure 4. Due to the kinematic loops in the mechanism, the device cannot fit on a single linkage sublaminates. Therefore the complete device requires two linkage sublaminates. Each linkage sublaminates consists of five layers: two outer cardboard layers for rigid links, a polyimide (Kapton) layer that forms the joints, and two adhesive layers made of double sided acrylic tape that bond these functional layers. In order to generate the two linkage sublaminates needed for the device, we need 11 layers: five layers per linkage sublaminates and a layer of adhesive that connects the two linkage sublaminates. The linkage sublaminates layers are first bulk micro-machined individually using a CO₂ laser (Universal Laser Systems, PL3.50) and a layup is formed

using pin alignment. Rigid links can be formed by retaining stiff material layers; likewise, hinges are defined by regions where the stiff cardboard is removed and polyimide is retained, allowing neighboring stiff regions to move relative to each other. To bond the two sublaminates together, an adhesive layer is defined by the intersecting geometries between neighboring sublaminates, forming islands of material which must be selectively added during the stacking procedure; a negative of this pattern is thus cut from polyimide film and used as a mask to selectively spray adhesive (3M Hi-Strength 90 Spray Adhesive) in the required pattern. The cut files for these all these geometries are automatically generated by popupCAD, which is able to account for any material which becomes obscured after lamination.

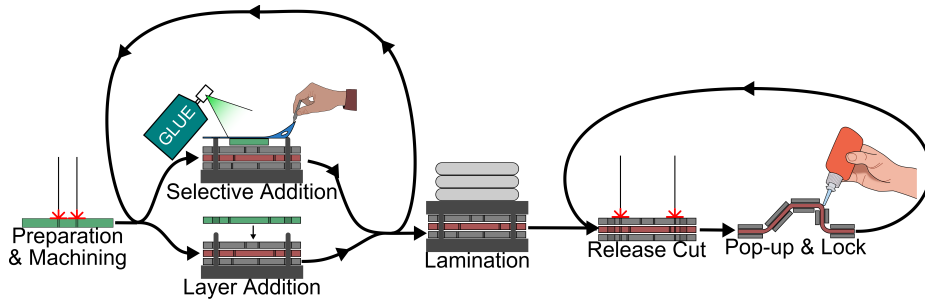


Fig. 4: The Device Fabrication Process.

4 Kinematics

| | | | | | | | | | | | | |
|------------|-------------|-------------|-------------|-----------|-------------|-------------|------------|-----------|-------------|-------------|-------------|----------|
| Frame | A_1 | B_1 | C_1 | D_1 | A_2 | B_2 | C_2 | D_2 | E_1 | F_1 | G_1 | H_1 |
| Parent | Base | A_1 | B_1 | C_1 | Base | A_2 | B_2 | C_2 | Base | E_1 | F_1 | G_1 |
| a | 0 | 0 | 0 | 0 | 0 | 0 | 0 | 0 | 1 | 0 | 0 | 0 |
| a_i | 0 | 0 | 0 | 0 | 0 | 0 | 0 | 0 | 0 | 0 | 0 | 0 |
| α_i | $-\pi/4$ | $\pi/4$ | $\pi/4$ | $-\pi/4$ | $-3\pi/4$ | $-\pi/4$ | $-\pi/4$ | $-3\pi/4$ | $-\pi/4$ | $\pi/4$ | $\pi/4$ | $-\pi/4$ |
| θ_i | $-q_{a1}^*$ | q_{b1}^* | $-q_{c1}^*$ | 0 | q_{a2}^* | $-q_{b2}^*$ | q_{c2}^* | 0 | $-q_{e1}^*$ | q_{f1}^* | $-q_{g1}^*$ | 0 |
| Frame | E_2 | F_2 | G_2 | H_2 | I_1 | J_1 | K_1 | L_1 | I_2 | J_2 | K_2 | L_2 |
| Parent | Base | E_2 | F_2 | G_2 | Base | A_1 | I_1 | K_1 | Base | A_2 | I_2 | K_2 |
| a | 1 | 0 | 0 | 0 | 1 | 0 | 0 | 0 | 1 | 0 | 0 | 0 |
| a_i | 0 | 0 | 0 | 0 | 0 | 0 | 0 | 0 | 0 | 0 | 0 | 0 |
| α_i | $-3\pi/4$ | $-\pi/4$ | $-\pi/4$ | $-3\pi/4$ | 0 | $-\pi/4$ | $-\pi/4$ | $-\pi/4$ | 0 | $-\pi/4$ | $-3\pi/4$ | $\pi/4$ |
| θ_i | q_{e2}^* | $-q_{f2}^*$ | q_{g2}^* | 0 | $-q_{i1}^*$ | q_{j1}^* | q_{k1}^* | 0 | $-q_{i2}^*$ | $-q_{j2}^*$ | $-q_{k2}^*$ | 0 |

* indicates state variable.

Table 1: Denavit-Hartenberg Parameters.

Four kinematic loops determine the transmission characteristics between the actuators and the leg. The two 6R spherical linkages establish one kinematic loop each, and the two 4R spherical linkages define two additional kinematic loops. One of the six-bar linkages is shown in Figure 2b. Frames $A_1, B_1, C_1, D_1, A_2, B_2, C_2,$ and D_2 belonging to this linkage can be used to generate the kinematic loop equations, which are generated by aligning the basis vectors of frames D_1 and D_2 using the equations

$$0 = \hat{x}_1 \cdot \hat{x}_2 - 1 \quad (1)$$

$$0 = \hat{y}_1 \cdot \hat{y}_2 - 1 \quad (2)$$

$$0 = \hat{z}_1 \cdot \hat{z}_2 - 1, \quad (3)$$

where x_1, y_1, z_1 and x_2, y_2, z_2 represent the orthonormal basis vectors for frames D_1 and D_2 , respectively. These three equations establish a relationship between the six state variables $q_{a1}, q_{b1}, q_{c1}, q_{a2}, q_{b2},$ and q_{c2} , establishing that the output frame D_1 has three rotational degrees of freedom. Between the newtonian reference frame(the base frame) and D_1 , this mechanism can be treated as a spherical joint.

The second 6R spherical linkage consisting of frames $E_1, F_1, G_1, H_1, E_2, F_2, G_2,$ and H_2 behaves like the first, establishing the spherical loop constraint equations between H_1 and H_2 using Equations (1-3). The outputs of the two 6R spherical linkages are connected by a 2R linkage which enforces orientation between the frames D_1 and H_1 using Equations (1-3) and

$$0 = (\hat{n}_y \times \hat{d}_{1z}) \cdot (\hat{n}_y \times \hat{d}_{1z}) - 1, \quad (4)$$

where n_z represents the z-oriented basis vector of the Newtonian reference frame. Figure 5 highlights the output degrees of freedom produced by the above constraint equations. The six-bar linkages have been replaced with equivalent spherical joints and input links have been omitted for clarity.

The two 4R spherical linkages, defined by the frames $\{A_1, I_1, J_1, K_1\}$ and $\{A_2, I_2, J_2, K_2\}$ respectively, are used to transmit the linear forces from each piezo-electric actuator into frames A_1 and A_2 of the bottom 6R spherical linkage. Frames J_1 and J_2 are aligned with K_1 and K_2 respectively using Equations (1-3). Thus for the four kinematic loops, 10 constraint equations can be established for the 12 state variables, establishing a two degree-of-freedom system.

Using the principle of virtual work, two Jacobians of the constraint equations may be obtained for the independent and dependent state variables by taking the partial derivative of the vector of constraint equations $\mathbf{f}(q)$ with respect to to each variable in \mathbf{q}_{ind} and \mathbf{q}_{dep} to obtain \mathbf{J}_{ind} and \mathbf{J}_{dep} , respectively. Two state variables must be selected for the independent state vector, so in this case we pick $\mathbf{q}_{ind} = [q_{i1}, q_{i2}]^T$. The rest are put in \mathbf{q}_{dep} . The Jacobians can then be

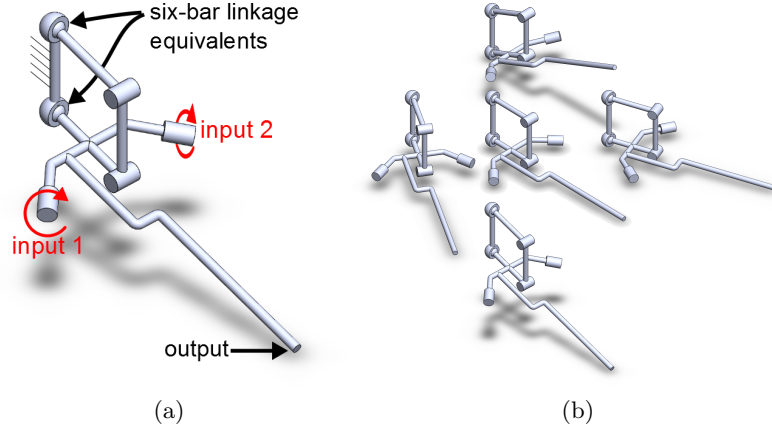


Fig. 5: An equivalent leg mechanism. In (a), the output stage of the leg is represented by spherical and revolute joints. Input linkages are omitted for clarity. In (b), the two degrees of freedom are highlighted by a variety of leg positions.

derived according to

$$0 = J_{ind}\dot{\mathbf{q}}_{ind} + J_{dep}\dot{\mathbf{q}}_{dep}, \quad (5)$$

$$-J_{dep}\dot{\mathbf{q}}_{dep} = J_{ind}\dot{\mathbf{q}}_{ind}, \text{ and} \quad (6)$$

$$\dot{\mathbf{q}}_{dep} = \underbrace{-J_{dep}^{-1}J_{ind}}_T \dot{\mathbf{q}}_{ind}. \quad (7)$$

The position of the actuator input and leg output can be represented in terms of the independent and dependent state variables \mathbf{q}_{ind} and \mathbf{q}_{dep} , respectively. This permits the calculation of input and output Jacobians as

$$\dot{\mathbf{q}}_{in} = A\dot{\mathbf{q}}_{ind} + B\dot{\mathbf{q}}_{dep} \quad (8)$$

$$\dot{\mathbf{q}}_{out} = C\dot{\mathbf{q}}_{ind} + D\dot{\mathbf{q}}_{dep}. \quad (9)$$

By combining Equations (7-9), a direct relationship between input and output velocities can be determined, as

$$\dot{\mathbf{q}}_{in} = \underbrace{(A + BT)}_E \dot{\mathbf{q}}_{ind} \quad (10)$$

$$\dot{\mathbf{q}}_{out} = \underbrace{(C + DT)}_F \dot{\mathbf{q}}_{ind} \quad (11)$$

$$\dot{\mathbf{q}}_{out} = FE^{-1}\dot{\mathbf{q}}_{in}. \quad (12)$$

These equations permit the calculation of the input/output transmission ratios and the resulting output path as a function of a valid initial state, as shown in Figure 6.

5 Discussion

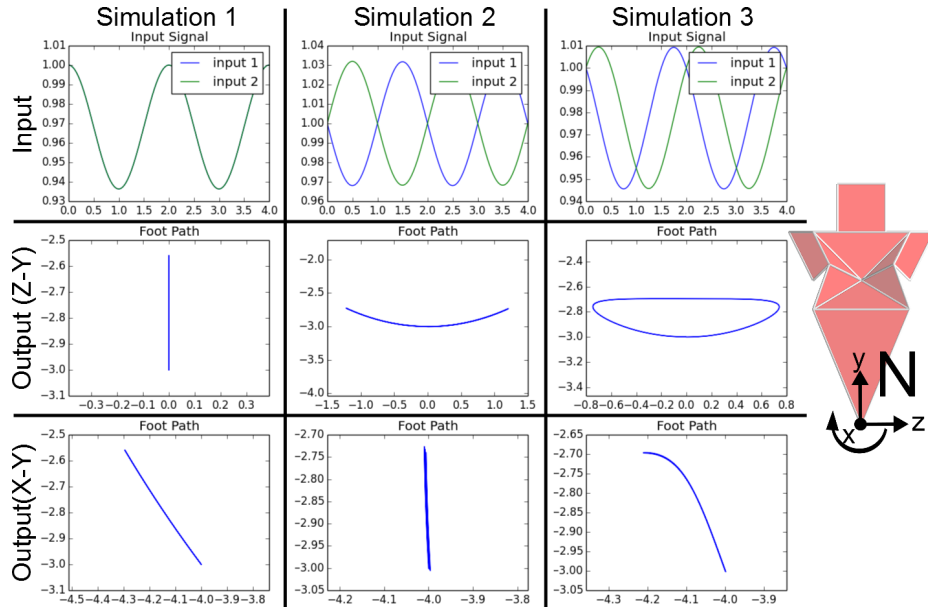


Fig. 6: Transmission Plots for three different input signals. In the first simulation, inputs are driven in phase, highlighting the lift degree of freedom. In the second simulation, a phase shift of π is used to highlight the swing degree of freedom. In the third simulation, a phase shift of $\pi/2$ shows a more-circular foot path typical of that likely to be used during walking. In these simulations, the x-axis is into the page.

A motion study has been performed for the constrained mechanism, determining output trajectories and velocities as a function of actuator input signal. A variety of input signals were tested, with the results from three simulations shown in Figure 6. As can be seen in the plots of the three simulations, driving the signals in phase with each other produces lift motion in the leg (along \hat{n}_y), and differential signals produce swing motion (motion along \hat{n}_z). By supplying combinations of input and phase offset, a variety of trajectories can be produced, as seen in the third simulation of Figure 6.

6 Future Work

Several initial prototypes were constructed in order to understand the kinematics of this rather non-intuitive device. While these prototypes were useful for confirming the basic kinematics of the device, they were not ideal in terms of

their hinges' functionality. This is due to the large gap between rigid elements, as well as to the non-zero thickness of the stacked cardboard, kapton, and adhesive. Future prototypes will be constructed with the materials used in the PC-MEMS paradigm, which will allow these hinges to perform more ideally. At that point, a full characterization of leg kinematics will be performed.

In addition, while the leg design presented in this paper utilizes concepts often seen in biology, we have not yet optimized it to match any biological system seen in nature. This will occur later in the design process, at which point it will accompany a much more in-depth performance analysis.

7 Conclusions

In this paper we have presented the initial design and kinematic evaluation for a bio-inspired leg transmission, suitable for integration into new crawling robot designs. Work is continuing in this direction, both on leg design and integration issues. While this transmission offers similar capabilities to the legs employed in current-generation legs, it offers the additional compatibility with monolithic assembly methods which can help reduce errors during assembly and speed up the process. As design criteria for these new robots become more developed, the models developed here can become the basis for further design and optimization of the transmission. In particular, the study of the dynamics of this new device will be crucial in evaluating and comparing current and future designs. In addition, by deriving the inverse kinematics of the leg, complex custom foot trajectories may be generated as a function of the two actuators.

The mechanism presented in this work is also ideal for insect-inspired robots due to its size and two-degree-of-freedom output. Since the mechanism includes the actuators, transmission, and the leg in a single system, it can be considered modular; i.e. several of them can be connected together to form a quadruped, hexapod, or a centipede-inspired multi-legged modular robot. We plan to use the mechanism presented in a centipede-inspired modular robot in the near future.

References

1. Aukes, D.M., Goldberg, B., Cutkosky, M.R., Wood, R.J.: An Analytic Framework for Developing Inherently-Manufacturable Pop-up Laminate Devices. *Smart Materials and Structures* (to appear) (2014)
2. Baisch, A.T., Heimlich, C., Karpelson, M., Wood, R.J.: HAMR3: An autonomous 1.7g ambulatory robot. In: 2011 IEEE/RSJ International Conference on Intelligent Robots and Systems. pp. 5073–5079. IEEE (Sep 2011)
3. Baisch, A., Ozcan, O., Goldberg, B., Ithier, D., Wood, R.: High Speed Locomotion for a Quadrupedal Microrobot. *International Journal of Robotics Research* (2014)
4. Gollnick, P.S., Magleby, S.P., Howell, L.L.: An Introduction to Multilayer Lamina Emergent Mechanisms. *Journal of Mechanical Design* 133(8), 081006 (2011)
5. Hoffman, K.L., Wood, R.J.: Passive undulatory gaits enhance walking in a myriapod millirobot. In: 2011 IEEE/RSJ International Conference on Intelligent Robots and Systems. vol. 2, pp. 1479–1486. IEEE (Sep 2011)

6. Hoover, A.M., Fearing, R.S.: Fast scale prototyping for folded millirobots. 2008 IEEE International Conference on Robotics and Automation pp. 1777–1778 (May 2008)
7. Hoover, A., Steltz, E., Fearing, R.: RoACH: An autonomous 2.4g crawling hexapod robot. In: 2008 IEEE/RSJ International Conference on Intelligent Robots and Systems. pp. 26–33. IEEE (Sep 2008)
8. Jacobsen, J.O., Winder, B.G., Howell, L.L., Magleby, S.P.: Lamina Emergent Mechanisms and Their Basic Elements. *Journal of Mechanisms and Robotics* 2(1), 011003 (2010)
9. Sreetharan, P.S., Whitney, J.P., Strauss, M.D., Wood, R.J.: Monolithic fabrication of millimeter-scale machines. *Journal of Micromechanics and Microengineering* 22(5), 055027 (May 2012)
10. Whitney, J.P., Sreetharan, P.S., Ma, K.Y., Wood, R.J.: Pop-up book MEMS. *Journal of Micromechanics and Microengineering* 21(11), 115021 (Nov 2011)
11. Wood, R.J., Avadhanula, S., Sahai, R., Steltz, E., Fearing, R.S.: Microrobot Design Using Fiber Reinforced Composites. *Journal of Mechanical Design* 130(5), 052304 (2008)